Analysis of Leading-Edge Separation Bubbles on Airfoils

Peter Crimi* and Barry L. Reeves*
Avco Systems Division, Wilmington, Mass.

The small separation bubbles which form near the leading edge of airfoils prior to the onset of leading-edge stall have been analyzed in detail, including the effects of viscous-inviscid interaction. The separated laminar shear layer, transitional flow, and turbulent reattaching flow are represented by an integral formulation. A correlation of local shear-layer parameters has been developed for determining the onset of transition in the laminar shear layer. Solutions are obtained using an iterative procedure, with strong interaction effects limited to the immediate vicinity of the separation bubble. Five different cases are analyzed, varying both angle of attack and Reynolds number. Results are in good agreement with wind tunnel measurements.

Nomenclature

a = parameter characterizing similarity solution
c = airfoil chord
m = inclination of external flow, $m = v_e/u_e$
Re = Reynolds number, $Re = Uc/\nu$
U = magnitude of freestream velocity
u = component of fluid velocity parallel to airfoil surface
u_0 = value of u in the absence of viscous effects
$\bar{u}$ = perturbation caused by viscous effects, $\bar{u} = u_e/u_0 - 1$
v = component of fluid velocity normal to airfoil surface
x = coordinate along airfoil surface, with origin at the leading edge
y = coordinate normal to airfoil surface
α = angle of attack
δ = boundary-layer or shear layer thickness, value of y at which $u = 0.99\,u_e$
δ^* = boundary-layer or shear layer displacement thickness
ν = kinematic viscosity
σ = turbulent intermittancy function

Subscripts

e = external inviscid flow
L = laminar
s = separation
T = turbulent
t = transition

I. Introduction

THE regions of separated flow which form on airfoils govern the airfoil stall characteristics. The nature and extent of these regions are determined primarily by the airfoil shape, incidence, and Reynolds number. Of concern here are the small separation bubbles which form near the leading edge of airfoils of moderate thickness ratio (0.09 to 0.15) at chordal Reynolds numbers in the range from one to ten million. The occurrence of what is termed leading-edge stall, characterized by an abrupt loss in lift and increase in drag, can be attributed to the sudden breakdown, or bursting, of the leading-edge bubble.[1]

The flow in the vicinity of the leading edge of an airfoil subject to leading-edge stall is as sketched in Fig. 1. The laminar boundary layer, extending from the stagnation point over the leading edge, separates just downstream of the point of minimum pressure. Transition to turbulent flow occurs in the free shear layer a short distance downstream of the separation point. The flow then reattaches to the airfoil surface, with a turbulent boundary layer extending from the reattachment point to the trailing edge. If the angle of attack of the airfoil is increased, the bubble moves closer to the leading edge and becomes slightly shorter. The bubble has almost no effect on integrated loads, because it is never more than a few percent of the chord in length. In the immediate vicinity of the bubble, though, there is strong interaction between the viscous and inviscid flows.

The specific mechanism for bubble breakdown is not presently known. It has been postulated, though, that there is a physical limitation in the amount of pressure recovery possible in the turbulent shear layer, so the bubble bursts when the limit is exceeded and the shear layer fails to reattach. Alternatively, it has been suggested that stall results from spearation of the turbulent boundary layer just downstream of reattachment.[2] This study was undertaken to provide a tool for investigating the specific mechanism for breakdown of the leading-edge bubble and, ultimately, for accurately predicting the onset of leading-edge stall.

Leading-edge bubbles have been the subject of numerous studies. Reviews of this work are given in Refs. 2 and 3. The primary difficulties in treating the problem analytically derive from the interaction between the viscous and inviscid flows and the coupling between the interaction and transition from laminar to turbulent flow in the free shear layer. Analyses have been carried out using semi-empirical formulations which do provide fairly good qualitative agreement with tests in predicting stall onset.[4,5] However, the modeling has not been adequate for analyzing the details of the flow in and near the bubble.

More recently, separation bubbles which occur near midchord on relatively thick airfoils at zero incidence were analyzed numerically using a finite-difference method.[6] While these bubbles are about ten times longer than leading-edge bubbles, their structure is quite similar, with transition occurring in the free shear layer. The results of that analysis are in excellent agreement with the flow measurements reported in Ref. 7. It should be noted, in particular, that in Ref. 6 interaction was assumed to be limited to the vicinity of the bubble. Also, the validity of the boundary-layer approximation for analyzing the bubble was verified by direct comparison with a solution using the complete Navier-Stokes equations.

In this study, the separated and reattaching shear layer in a leading-edge bubble is analyzed using an integral formulation, assuming the boundary-layer approximation is applicable. Interaction between the viscous and inviscid flows in the vicinity of the bubble is taken into account through an iterative procedure. A key element of this analysis is the determination of the position of transition onset in the laminar shear layer.

Received April 22, 1976; revision received July 27, 1976. This study was supported by the U.S. Army Research Office under Contract No. DAHC04-74-C-0035.

Index categories: Subsonic and Transonic Flow; Jets, Wakes, and Viscous-Inviscid Interaction; Aircraft Aerodynamics.

*Senior Consulting Scientist. Member AIAA.

A correlation of local shear-layer parameters at transition was developed, using the data of Ref. 7. The correlation is based on an analogy between transition in separated shear layers and transition produced by two-dimensional roughness elements.[8]

The formulations of the inviscid and viscous flows and the transition model are given in Sec. II. The iteration procedure is then outlined. Results of calculations are presented and compared with measurements for leading-edge bubbles on an airfoil with thickness ratio of 0.10 at angles of attack of 8 and 12-deg and chordal Reynolds numbers of 2×10^6 and 3×10^6.

II. Representation of Flow Elements

Inviscid Flow

The flow is assumed to be two-dimensional and incompressible. Let $u_0(x)$ denote the magnitude of fluid velocity at the airfoil surface that would result in the absence of viscous effects. The flow component tangent to the airfoil surface at the interface of the viscous and inviscid flows is written in the form

$$u_e(x)=u_0(x)\ [1+\tilde{u}\ (x)] \tag{1}$$

A previously developed digital computer program[9] is employed in the analysis to direct the computation of u_0, given the airfoil shape and angle of attack, using a source distribution on the airfoil surface and a vortex distribution on the chord line.

The analyses of the boundary layer and shear layer provide the flow inclination v_e/u_e at the interface of the viscous and inviscid flows, which can be related to $\tilde{u}$ as follows. Interaction is taken to occur on the interval $x_A\le x\le x_B$, over which it is assumed the surface curvature is negligible. The perturbation to the inviscid flow is derived from a potential; the potential is formulated from a source distribution of strength μ on the airfoil surface. The components of the perturbation in the x and y directions, respectively, are then given by

$$u_p(x,y)=\frac{1}{2\pi}\int_{x_A}^{x_B}\frac{(x-\xi)\mu(\xi)\,d\xi}{(x-\xi)^2+y^2}$$

$$v_p(x,y)=\frac{y}{2\pi}\int_{x_A}^{x_B}\frac{\mu(\xi)\,d\xi}{(x-\xi)^2+y^2}$$

Assuming u_p/u_0 and v_p/u_0 are small,

$$v_e(x)\approx v_p(x,0)$$

$$=\frac{\mu(x)}{2}$$

and

$$u_0(x)\ \tilde{u}\ (x)\approx u_p(x,0)$$

$$=\frac{1}{\pi}\int_{x_A}^{x_B}\frac{v_e(\xi)\,d\xi}{x-\xi}$$

With $m(x)\equiv v_e/u_e\approx v_e/u_0$, the above singular integral can be manipulated to give

$$\tilde{u}\ (x)=\frac{1}{\pi}\int_{x_A}^{x_B}\frac{m(\xi)\,d\xi}{x-\xi} \tag{2}$$

Viscous Flow

The flow in the free shear layer and the boundary layer in the vicinity of the separation bubble are represented using the integral formulation developed in Ref. 10 for analyzing supersonic separated and reattaching laminar flows involving strong interaction with the inviscid flow. The relations have been generalized to account for continuous transition from laminar to turbulent flow in the free shear layer. Both the momentum integral (zeroth moment) and first moment of momentum of the boundary-layer equations are used, so that for laminar or fully turbulent flow the velocity profiles can be characterized by a single parameter which is not related to the local pressure gradient. The family of similar solutions for reversed flow found by Stewartson[11] is employed for analyzing the free shear layer. Turbulence production is introduced using an exponentially increasing intermittancy function, with the constant in the exponent determined from measurements taken in a free shear layer undergoing transition.[12]

A coupled pair of first-order, ordinary, nonlinear differential equations was derived, as outlined below, from the momentum equations. They have been formulated in such a way that they can be integrated continuously downstream, starting in the laminar boundary layer and continuing through the separation point, transition in the laminar shear layer, and reattachment of the turbulent shear layer. The dependent variables are the displacement thickness δ^* and a parameter, denoted a, characterizing the velocity profile. That parameter is defined as follows

$$a=\frac{\delta}{u_e}\left(\frac{\partial u}{\partial y}\right)_{y=0} \qquad \text{attached flow} \tag{3a}$$

$$a=\left(\frac{y}{\delta}\right)_{u=0} \qquad \text{separated flow} \tag{3b}$$

The integral across the boundary layer of the momentum equation and of that equation multiplied by u give, respectively,[10]

$$H\frac{d\delta^*}{dx}+\delta^*\frac{dH}{dx}+(2H+1)\frac{\delta^*}{u_e}\frac{du_e}{dx}=\left(\frac{\nu}{u_e\delta^*}\right)P_L \tag{4}$$

$$J\frac{d\delta^*}{dx}+\delta^*\frac{dJ}{dH}+3J\frac{\delta^*}{u_e}\frac{du_e}{dx}=\left(\frac{\nu}{u_e\delta^*}\right)R_L+\sigma K_\theta\overline{HR} \tag{5}$$

The turbulent wall shear in the bubble has been neglected. The quantity σ in Eq. (5) is the turbulent intermittancy function which, from Emmons' spot theory,[13] can be written in the form

$$\sigma=0,\ x<x_t;$$

$$=1-e^{-C_T(x-x_t)^2},\ x\ge x_t$$

The value of C_T was computed, using the measured distance from transition onset to fully developed turbulent flow in a separation bubble given in Ref. 12, with the result that

$$C_T=0.025/\delta_s^{*2}$$

The other quantities in Eqs. (4) and (5) are defined as follows

$$\delta^*=\int_0^\delta\left(1-\frac{u}{u_e}\right)dy,\quad \theta=\int_0^\delta\frac{u}{u_e}\left(1-\frac{u}{u_e}\right)dy,$$

$$\theta^*=\int_0^\delta\frac{u}{u_e}\left(1-\frac{u^2}{u_e^2}\right)dy,\quad H=\theta/\delta^*,\quad J=\theta^*/\delta^*,$$

$$R_L=\frac{2\delta^*}{u_e^2}\int_0^\delta\left(\frac{\partial u}{\partial y}\right)^2dy,\qquad P_L=\frac{\delta^*}{u_e}\left(\frac{\partial u}{\partial y}\right)_{y=0}$$

$$K_\theta\overline{HR}=2\int_0^\delta\frac{\tau}{\rho u_e^2}\frac{\partial(u/u_e)}{\partial y}dy,\quad K_\theta=\frac{\epsilon}{u_e\theta},\quad \tau=\rho\epsilon\frac{\partial u}{\partial y}$$

where ϵ is the eddy viscosity. To complete the basic formulation, the continuity equation provides the following relation for flow inclination at the edge of the layer

$$v_e/u_e = \frac{d\delta^*}{dx} - Z\frac{\delta^*}{u_e}\cdot\frac{du_e}{dx} \tag{6}$$

where

$$Z = \frac{1}{\delta^*}\int_0^\delta \frac{u}{u_e}\,dy$$

Now, it is assumed that the quantities H, J, P, R, and Z are all known functions of parameter a alone. Thus, dH/dx can be replaced by $(dH/da)\ (da/dx)$ in Eqs. (4) and (5), making those relations a coupled pair of ordinary differential equations which can be solved, by direct numerical integration, for the dependent variables δ^* and a.

The dependence of H, J, etc. on a is complicated somewhat by the transition from laminar to turbulent flow. It is assumed, first, that H can be written in the form

$$H = (1-\sigma)H_L(a) + \sigma H_T(a)$$

and similarly for J and Z. The contributions of P_L and R_L in the reattaching turbulent shear layer are small compared to competing terms, so their values for a laminar profile are used throughout.

Guided by what has been observed in experiments involving turbulent free shear layers,[14-16] the turbulent velocity profile is assumed to vary continuously from a turbulent equilibrium profile[17] at reattachment, where $a=0$, to a laminar shear layer profile as a approaches unity. Thus, H_T is assumed to be of the form

$$H_T = \left(\frac{H_{S_T}}{H_{S_L}}\right) H_L(a) + f_T(a)\left(1-\frac{H_{S_T}}{H_{S_L}}\right)H_L(a)$$

where H_{S_T} and H_{S_L} are the values of H_T and H_L, respectively, at separation or reattachment ($H_{S_T}=0.429$, $H_{S_L}=0.247$), while $f_T(a)$ is a function which is zero at $a=0$ and asympotically approaches unity as a increases. The derivation of f_T will be described subsequently. The functions J_T and Z_T are defined similarly to H_T, with $J_{S_T}=0.654$, $Z_{S_T}=1.82$, $J_{S_L}=0.374$, $Z_{S_L}=1.035$. Substituting for H_T and J_T in the expressions for H and J, it is found that

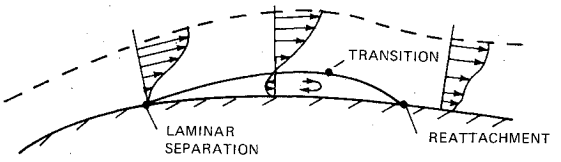

Fig. 1 Flow in the vicinity of the leading-edge bubble.

$$H = \left\{1+\sigma\left(\frac{H_{S_T}}{H_{S_L}}-1\right)\left[1-f_T(a)\right]\right\} H_L(a) \tag{7a}$$

$$J = \left\{1+\sigma\left(\frac{J_{S_T}}{J_{S_L}}-1\right)\left[1-f_T(a)\right]\right\} J_L(a) \tag{7b}$$

and similarly for Z. As noted previously, the variations of H_L, J_L, etc. with a are uniquely determined from the similarity solutions. The polynomial approximations obtained by least-square fits given in Ref. 18 were used for this analysis. The coefficients of those polynomials are listed in Table 1.

The differential equations used to analyze the viscous flow were obtained by substituting Eqs. (7) into Eqs. (4) and (5) and solving for the derivatives of δ^* and a. Since J_{S_T}/J_{S_L} and H_{S_T}/H_{S_L} differ by less than one percent, the value of the latter ratio was used for both ratios, which resulted in considerable simplification of the equation for a. The equations obtained are

$$\frac{d\delta^*}{dx} = \frac{1}{\mathfrak{D}}\left\{\frac{\nu}{u_e\delta^*}(C_J P - C_H R) - C_H\sigma K_\theta \overline{HR}\right.$$
$$+3\left[J_L C_H - C_J(2\beta H_L+1)\right]\frac{\delta^*}{u_e}\frac{du_e}{dx}$$
$$\left.+0.7361\frac{dH_L}{da}\left(J_L - H_L\frac{dJ_L}{dH_L}\right)\left[1-f(a)\right]\delta^*\frac{d\sigma}{dx}\right\} \tag{8}$$

$$\frac{da}{dx} = \frac{H_L}{\delta^*\mathfrak{D}}\left\{\frac{\nu}{u_e\delta^*}\left(R-\frac{J_L P}{H_L}\right)\right.$$
$$\left.+J_L\left(\frac{1}{H_L}-\beta\right)\frac{\delta^*}{u_e}\frac{du_e}{dx}+\sigma K_\theta\overline{HR}\right\} \tag{9}$$

Table 1 Coefficients of functions $\mathfrak{F} = \sum_{k=0}^{7} c_k a^k$

Function	c_0	c_1	c_2	c_3	c_4	c_5	c_6	c_7
				Attached profiles				
H_L	0.24711	0.11056	−0.02122	0.00435	−0.00097	0.000099		
J_L	0.37372	0.16969	−0.02336	0.00572	−0.00175	0.000191		
Z_L	1.03539	0.48373	−0.01502	0.02610	−0.00370			
R_L	1.25782	−0.55550	0.31964	−0.09077	0.01938	−0.000935		
P_L		0.48745	−0.09927	0.00960	−0.00031			
dH_L/da	0.11056	0.04245	0.01304	−0.00389	0.00050			
dJ_L/dH_L	1.50031	0.28105	−0.04287	0.00262				
				Separated profiles				
H_L	0.24711	−0.25057	−0.43012	0.1430	−0.4267	−10.8587	38.7425	−31.209
J_L	0.37372	−0.42859	0.33036	−5.1517	10.5964	−5.8174		
Z_L	1.03539	−1.02605	−1.12405	−1.1456	3.3434			
R_L	1.25782	1.09008	7.01736	−33.8762	196.7688	−371.9762	244.3095	
P_L		−1.19450	−0.70990	−7.1253	20.8568	−100.2729	310.2394	−263.587
dH_L/da	−0.25057	−0.86024	0.42888	−1.7068	−54.2937	232.4533	218.4644	
dJ_L/dH_L	1.50031	−0.84045	3.32376	−13.8668	5.4767	30.1770		

where

$$\beta = 1 + 0.7361[1 - f_T(a)]$$

$$\mathfrak{D} = \frac{dH_L}{da}\left(H_L \frac{dJ_L}{dH_L} - J_L\right)$$

$$C_J = \frac{dJ_L}{dH_L}\frac{dH_L}{da} - 0.7361\frac{\sigma J_L}{\beta}\frac{df_T}{da}$$

$$C_H = \frac{dH_L}{da} - 0.7361\frac{\sigma H_L}{\beta}\frac{df_T}{da}$$

To provide a physical basis for the derivation of f_T, it was observed that the velocity profile in the outer part of the turbulent separated shear layer in the tests of Ref. 16 had developed an essentially laminar form at a distance of approximately 12 δ_s from the separation point. Therefore, if Eqs. (8) and (9) are employed to analyze a fully turbulent free shear layer subjected to zero pressure gradient, the solution should be such that f_T is nearly unity – say, 0.95 – at that same distance from separation. Moreover, for the solution to be continuous, it is necessary that f_T', as well as f_T, be zero at $a = 0$. With f_T given by

$$f_T = 1 - \exp\left(\frac{-k_T a^2}{1-a}\right)$$

which meets the requirements at $a = 0$ and $a = 1$, solutions of Eqs. (8) and (9) for a turbulent free shear layer gave $k_T = 10$ for f_T equal to 0.95 at a distance of 12 δ_s from separation. This value of k_T was used in obtaining all subsequent solutions.

It should be noted that Eqs. (8) and (9) are singular in the vicinity of separation and reattachment (i.e., near $a = 0$) if $u_e(x)$ is prescribed. The singularities are removed by accounting for the viscous-inviscid interaction, through adjustment of the variation of du_e/dx, to yield finite derivatives of δ^* and a. The details of the procedure employed are outlined in the discussion of the iteration method.

Transition Onset

The mechanism for transition caused by an element of surface roughness is similar to what occurs in a leading-edge bubble. The flow separates locally at the roughness element and reattaches downstream. Because the initially laminar separated shear layer is much less stable than an attached boundary layer, transition may be triggered in the separated region. Because of this similarity, a correlation for transition in a leading-edge bubble is postulated which employs parameters analogous to those governing transition due to roughness. Specifically, Tani and Sato[8] found that test data for transition produced by roughness elements could be correlated in the form

$$(u_e\delta/\nu)_t = f(k/\delta_s^*)$$

where k is the height of the roughness element. It is assumed that the height of the $u = 0$ curve in the leading-edge bubble (i.e., $a_t\delta_t$) is the length scale which controls transition and is analogous to k. It became apparent from preliminary calculations, though, that the Reynolds number must be based on conditions at separation, rather than at transition. Thus, a relation of the form

$$(u_e\delta^*/\nu)_s = f(a_t\delta_t/\delta_s^*)$$

is postulated for correlating transition onset location in the bubble.

Using the measured pressure distributions given in Ref. 7, Eqs. (8) and (9) were integrated through separation and into the laminar free shear layer to provide streamwise variations of a. A total of 15 cases were analyzed, including leading-edge bubbles on two different airfoils, each at two different angles of attack, for freestream Reynolds numbers ranging from 1.5×10^6 to 6×10^6. For each case, the measured location of transition given in Ref. 7 was used to obtain the appropriate value of $a_t\delta_t/\delta_s^*$. For example, consider the solution obtained for an airfoil with a 0.10 thickness ratio at 12 deg angle of attack and a chordal Reynolds number of 3×10^6. Measured transition was at a distance of $0.0048c$ from separation. It was assumed that, at the measured location, transition had developed to the extent that σ had a value of 0.75.† Using the exponential formula for σ, the location of transition onset can be computed, giving $x_t - x_s = 0.0038c$. The values of a_t and δ_t at this location were obtained from the analysis of the laminar shear layer.

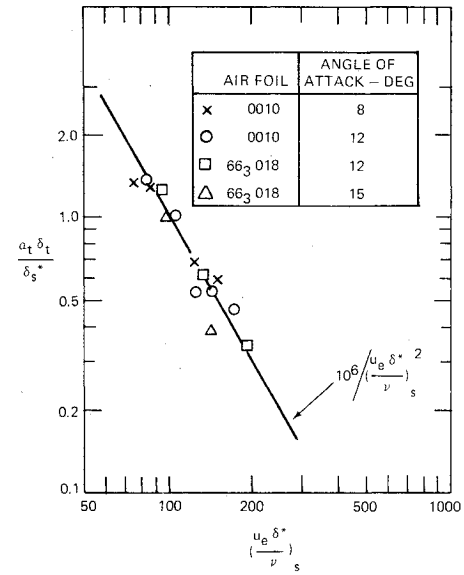

Fig. 2 Correlation of shear layer parameters at transition onset.

The results obtained are plotted in Fig. 2. While there is some scatter, particularly at the higher Reynolds numbers, the data are still well correlated by the postulated relation. The line drawn through the points is a plot of the simple relation

$$a_t\delta_t/\delta_s^* = 10^6/(u_e\delta^*/\nu)_s^2 \qquad (10)$$

which is seen to provide a quite good approximation to the derived correlation. This equation was used in the bubble analyses to locate transition onset, by continuously evaluating $a\delta/\delta_s^*$ during the integration of Eqs. (8) and (9) in the laminar shear layer, and comparing its value to that of the right-hand side of Eq. (10).

It should be noted that the data used for the correlation of Fig. 2 were all obtained for a relatively low freestream turbulence level of 0.15 to 0.2%, so the correlation, in its present form, is not applicable for relatively high freestream turbulence levels. The correlation could presumably be generalized to account for the effects of freestream turbulence, however.

III. Method of Analysis

Preliminary Calculations

To analyze the leading-edge bubble for specified airfoil section, angle of attack, and Reynolds number, the nominal inviscid flow $u_0(x)$ is first calculated using the previously

†It was intended to vary this value for σ parametrically. Since preliminary analyses of bubbles agreed well with measurements, however, it was decided that the initial value selected was satisfactory.

described computer program. A subprogram for directing the analysis of the laminar boundary layer starting from the forward stagnation point using the method of finite differences was incorporated in the program when it was developed. It was found convenient to employ that subprogram to analyze the laminar boundary layer over the surface to the vicinity of the minimum pressure point to provide initial conditions for the integral formulation of the viscous flow. The two analyses are connected by requiring continuity of displacement and momentum thicknesses.

Analysis of the Viscous Flow

The integration of Eqs. (8) and (9) proceeds from near the point of minimum pressure, given the initial values of x, δ^*, and a, and the functions u_e' and u_e. The Runge-Kutta method is used. The way in which u_e' and u_e are evaluated plays a role in the iteration process, so this will be described in some detail. The values of u_e' are specified at, say, N points, located by $x_1, x_2, \ldots, x_N$. It is assumed that u_e' is continuous and varies linearly between these points so that, if $x_i \le x \le x_{i+1}$,

$$u_e'(x) = u_e'(x_i) + [u_e'(x_{i+1}) - u_e'(x_i)] \frac{(x-x_i)}{(x_{i+1}-x_i)}$$

The value of u_e is obtained by direct integration of the above expression, so u_e varies parabolically between the specified points and is continuous with a continuous slope over the whole interval from x_1 to x_N. The functions u_e' and u_e are thus defined by specifying N values of u_e', N corresponding values of x, and the value of u_e at the first value of x.

The integration is divided into four parts, with divisions at the singularity just upstream of separation, at the point of transition onset, and at the singularity just downstream of reattachment. A different table of u_e' values is used for each of these parts. The tables for the laminar and turbulent boundary layers are constructed to yield the nominal flow (i.e., u_0) in those regimes, while the other tables are set up from the results of the previous iteration.

The integration proceeds from the starting point in the laminar boundary layer unitl a is less than 0.7 (about 10 displacement thicknesses upstream of the singularity). An estimate is then made of the value of u_e' needed at the singular point to make δ^* and a continuous there. The u_e' table is then reset so that u_e' varies linearly from its current value where $a = 0.7$ to the required value at the singular point. Just upstream of the singularity, the numerical integration is interrupted, and analytic solutions for δ^*, a, u_e', and u_e, developed from Taylor series expansions, are used over a small interval containing the singularity. The numerical integration is then restarted, using the u_e' table for the laminar shear layer, after the first entry in that table is adjusted to make it agree with the analytic solution for u_e'. Integration then proceeds until transition onset, as determined by the previously described correlation, at which point the u_e' table for the transitional and turbulent shear layer is used. The two u_e' tables for the shear layer are simply obtained by dividing the result obtained from the last iteration at the point of transition onset. If transition has not occurred when the end of the table for the laminar shear layer is reached, the integration continues using the last value in the u_e' table. This division is necessary because the steep gradients in u_e downstream of transition for the previous step would prevent transition from occurring altogether if it is delayed a small distance past the transition point of the previous step.

Integration then proceeds to the point of turbulent reattachment, which is just upstream of the other singular point. The same procedure as was used at the singularity near separation is employed to bridge the one near reattachment, starting with a preliminary adjustment of the u_e' table and ending just downstream of the singularity with an analytic solution. It is then assumed that u_e' varies linearly from its value there to u_0' at a distance of about 15 displacement thicknesses from the singularity, and numerical integration proceeds out to just beyond the point where $u_e' = u_0'$, completing the viscous-flow analysis.

Derivation of Inviscid Flow to Account for Interaction

An iteration step is completed by obtaining revised estimates of u_e' and u_e as dictated by the relations governing the viscous-inviscid interaction. The obvious procedure of simply substituting the variation of v_e/u_e obtained from the viscous-flow analysis, Eq. (6), into the integrand of Eq. (2) was found to be unsuitable. The initial estimate for the u_e' variation inevitably produces small but physically unrealistic excursions in δ^* in the immediate vicinity of transition, which cause rapid divergence of results for successive iterations. The following procedure was therefore devised.

The interaction is introduced using the differential equation for δ^*, Eq. (8), as a link to the variation of δ^* obtained in the analysis of the viscous flow. Specifically, a and δ^* are regarded, for this purpose, as known functions in that equation, while $\delta^{*\prime}$ and u_e' are regarded as unknown but related through Eqs. (2) and (6). It is then possible to formulate a linear equation which can be solved for u_e'. The basic unknown for this calculation is assumed to be the flow inclination $m(x)$ over the interval between the two singularities. It is further assumed that m has the value computed from the viscous-flow analysis at each of these singularities. The function m is then cast in the form

$$m(\phi) = \sum_{n=1} A_n \sin n\phi + m_{UL}(\phi) \tag{11}$$

where ϕ varies between 0 and π on the interval between the upstream singularity at $x = x_U$ and the downstream one at $x = x_L$

$$\cos\phi = 1 - 2(x-x_U)/(x_L-x_U), \quad x_U \le x \le x_L$$

The A_n's are unknown coefficients and m_{UL} is a known function which imparts the proper values to m at the end points

$$m_{UL} = m(x_U)\left[1-\left(\frac{x-x_U}{x_{x_L}-x_U}\right)\right]^2\left\{1+K_U(x-x_U)\right\}$$

$$+ m(x_L)\left(\frac{x-x_U}{x_L-x_U}\right)^2\left\{1-K_L\left[1-\left(\frac{x-x_U}{x_L-x_U}\right)\right]\right\}$$

The constants K_U and K_L are assigned to make the derivative of m_{UL} match that computed at the singularities as well, for a reason which will be evident subsequently.

Now, the inviscid-flow perturbation $\tilde{u}$ is obtained from Eq. (2), with m defined by Eq. (11) between the singularities. Upstream and downstream boundary-layer displacement effects are taken into account as well by directly substituting the variation of m obtained from the viscous-flow analysis for those regions in Eq. (2). It is found, then, that $\tilde{u}$ over the bubble is given by

$$\tilde{u} = -\sum_{n=1} A_n \cos n\phi + \tilde{u}_{UL} + \tilde{u}_{BL} \tag{12}$$

where

$$\tilde{u}_{UL} = \frac{1}{\pi} \int_{x_U}^{x_L} \frac{m_{UL}(\xi)\,d\xi}{x-\xi}$$

and $\tilde{u}_{BL}$ is the contribution of the segments of boundary layer adjacent to the bubble.

It was necessary to make the derivative of m_{UL} match the viscous-flow result at the singularities so that the sum $\tilde{u}_{UL} + \tilde{u}_{BL}$ would be well behaved at those points. If the derivative of m_{UL} were not continuous, Eq. (12) would yield logarithmic singularities in $\tilde{u}$ at x_U and x_L.

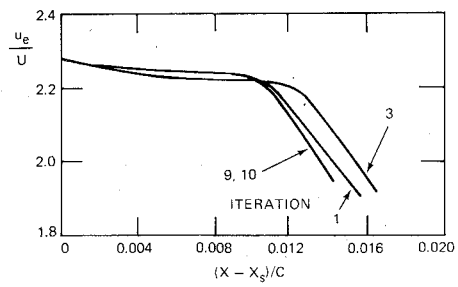

Fig. 3 Assumed, intermediate, and final solutions for u_e: $\alpha = 8$ deg, $Re = 2 \times 10^6$.

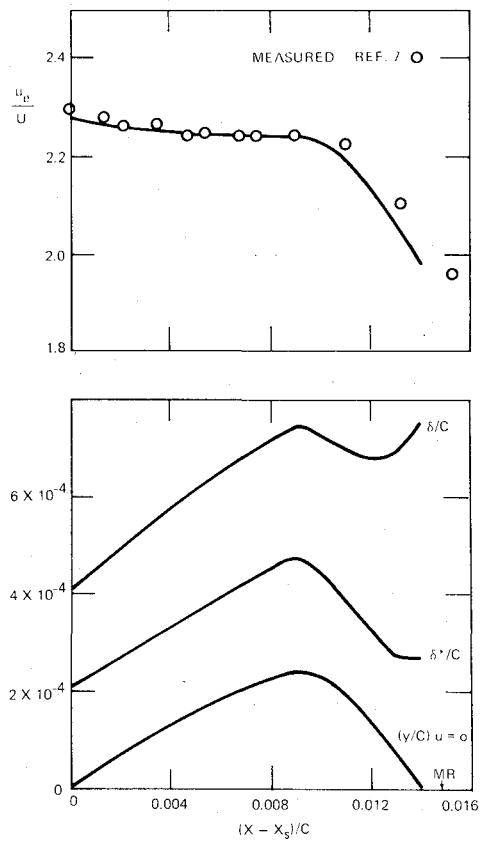

Fig. 4 Results for 0010 airfoil: $\alpha = 8$ deg, $Re = 2 \times 10^6$.

It should be noted here that the contribution of the interaction from the adjacent boundary layers is small, the results being quite insensitive to the extent of boundary layer used in calculating $\bar{u}_{BL}$. Including these effects was necessary, however, because it insured continuity of the solution for $\bar{u}$ at x_U and x_L.

Next, in preparation for substituting Eqs. (11) and (12) into Eq. (8), it is noted, from Eq. (6), that

$$d\delta^*/dx = m(\phi) + (Z\delta^*/u_e)\ du_e/dx$$

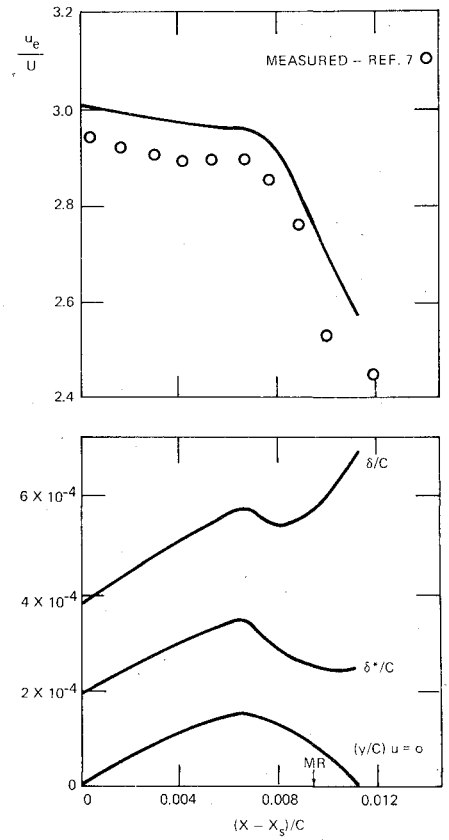

Fig. 5 Results for 0010 airfoil: $\alpha = 12$ deg, $Re = 2 \times 10^6$.

and that, to first order

$$(1/u_e)\ du_e/dx = u_0'/u_0 + \bar{u}', \quad 1/u_e = (1-\bar{u})/u_0$$

Combining these expressions with Eqs. (11) and (12) and substituting into Eq. (8), then,

$$\sum_{n=1} A_n \sin n\phi + m_{UL} + Z\delta^* \left[\frac{u_0'}{u_0} + \bar{u}_{UL}' + \bar{u}_{BL}' + \frac{2}{(x_L - x_U)\sin\phi} \sum_{n=1} nA_n \sin n\phi \right] = \frac{1}{\mathfrak{D}} \left\{ \frac{\nu}{u_0 \delta^*} (C_J P - C_H R)(1 + \sum_{n=1} A_n \cos n\phi - \bar{u}_{UL} - \bar{u}_{BL}) - C_H K_\theta \overline{HR} \right. \quad (13)$$

$$+ \left[3\beta J_L C_H - C_J (2\beta H_L + 1) \right] \delta^* \left[\frac{u_0'}{u_0} + \bar{u}_{UL}' + \bar{u}_{BL}' + \frac{2}{(x_L - x_u)\sin\phi} \sum_{n=1} nA_n \sin n\phi \right]$$

$$\left. + 0.7361 \frac{dH_L}{da} \left[J_L - H_L \frac{dJ_L}{dH_L} \right] [1 - f_T(a)]\, \delta^* \frac{d\sigma}{dx} \right\}$$

Table 2 Comparison of computed and measured separation location and boundary- layer thickness at separation

Airfoil section	α, deg	Re, $\times 10^{-6}$	x_s/c Measured	x_s/c Computed	$10^4 y/c$ for $u = 0.707\, u_{e_s}$ Measured	$10^4 y/c$ for $u = 0.707\, u_{e_s}$ Computed
0010	8	2	0.022	0.0201	2.33	2.51
0010	8	3	0.022	0.0200	1.90	2.05
0010	12	2	0.0167	0.0157	1.83	2.29
0010	12	3	0.0167	0.0153	1.49	1.74
63-009	7	5.8	0.0078	0.0088	–	1.08

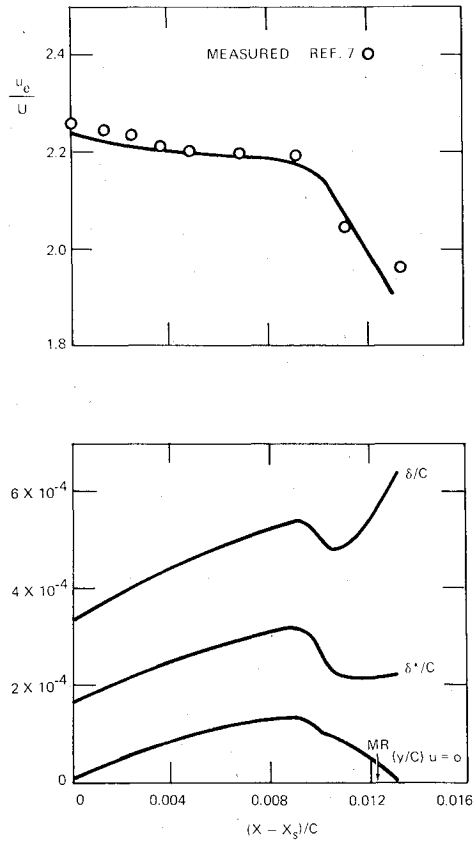

Fig. 6 Results for 0010 airfoil: $\alpha = 8$ deg, $Re = 3 \times 10^6$.

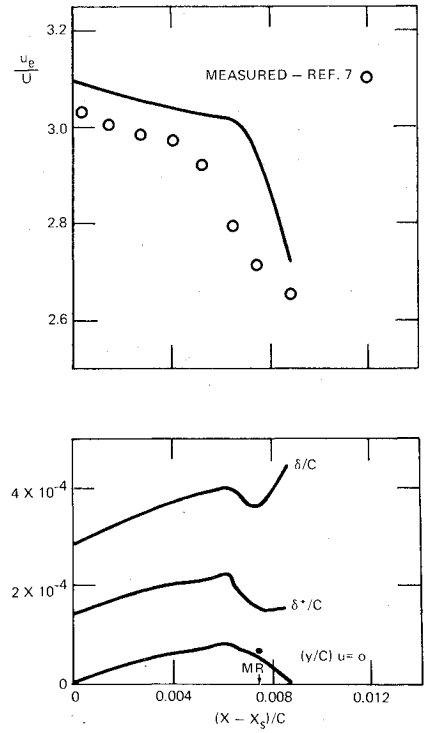

Fig. 7 Results for 0010 airfoil: $\alpha = 12$ deg, $Re = 3 \times 10^6$.

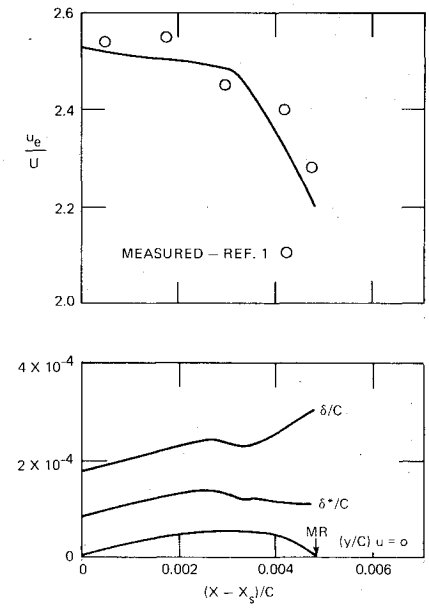

Fig. 8 Results for 63-009 airfoil: $\alpha = 7$ deg, $Re = 5.8 \times 10^6$.

In Eq. (13), δ^* and σ, where they appear explicitly, and all explicit functions of a, are regarded as known functions defined by the latest solution of Eqs. (8) and (9) for δ^* and a. A set of linear algebraic equations for the coefficients A_n is derived from Eq. (13) by the following procedure. All series involving the A_n's are truncated after N_f terms (N_f was made 20 for all calculations); Eq. (13) is multiplied through by $\sin\phi \sin K\phi$, $K = 1,2,\ldots, N_f - 2$; and the result is integrated from $\phi = 0$ to $\phi = \pi$. The remaining two equations needed are obtained by requiring that the solution be continuous at the singularities. That is, the expression in curly brackets on the right-hand side of Eq. (13) is set equal to zero for $\phi = 0$ and for $\phi = \pi$. The resulting set of N_f equations is solved by the method of successive elimination of unknowns.

Iteration Procedure

After performing the preliminary calculations, an initial estimate of the variation of u_e' over the bubble is made. The viscous flow is then analyzed, and a solution for u_e' obtained from the interaction calculation to complete the first iteration. A weighted average of the interaction result and the u_e' variation used in the viscous-flow analysis is then employed in the next and successive iterations to again analyze the viscous flow. The rate of convergence of this procedure is very sensitive to what fraction is used in the weighted averaging. It was found that taking 80% of the previous variation in u_e' in each step gave the best results.

Representative results for one of the cases analyzed are shown in Fig. 3. The bubble analyzed was on an airfoil with a 0.10 thickness ratio at 8 deg angle of attack and a Reynolds number of 2×10^6. The u_e variations between separation and reattachment for four of the ten iterations are plotted in the figure. The farthest downstream excursion in the point of transition onset was in the third iteration. Solutions for the ninth and tenth iterations were nearly identical, so only a single curve is drawn.

IV. Results of Computations

Four cases were analyzed, using the airfoil section of the modified NACA 0010 airfoil for which test results are reported in Ref. 7. The leading-edge bubble was analyzed for angles of attack, α, of 8 and 12 deg., for chordal Reynolds numbers of both 2×10^6 and 3×10^6 at each angle of attack. To verify that the model is generally applicable, a fifth case was analyzed for comparison with data which were not employed in the transition correlation. Specifically, the leading-edge bubble on an NACA 63-009 airfoil at a Reynolds number of 5.8×10^6, with $\alpha = 7$ deg., was analyzed for comparison with the data of Ref. 1. Solutions for the 0010 airfoil were obtained after a maximum of eleven iterations, the case with $\alpha = 12$ deg. and $Re = 3 \times 10^6$ being the slowest to converge.

The solution for the 63-009 airfoil required 23 iterations. The computed and measured distances to separation and boundary layer thickness (value of y for $u = 0.707\ u_e$, as defined in Ref. 7) at separation are given in Table 2.

The results of the bubble analyses for the five cases are plotted in Figs. 4 through 8. The variations between separation and reattachment of u_e, boundary-layer thickness δ (value of y for $u = 0.99\ u_e$), displacement thickness δ^*, and the ordinate where $u = 0$, are plotted in those figures. The measured location of reattachment is marked on the abscissa by a small arrow. The agreement between the computed and measured variations of u_e is seen to be very good. The analytical results for the two cases with $\alpha = 12$ deg (Figs. 5 and 7) is about 3% higher than the measured u_e, because the computed separation point was upstream of the measured one (see Table 2), making the u_e at separation slightly higher. The predicted locations of transition onset and the streamwise velocity gradients both upstream of transition and during pressure recovery all agree well with the test results, however.

It is seen by comparing the measured and computed reattachment points that bubble length is also well predicted. As a result, the expected effects of variations in angle of attack and Reynolds number are apparent; i.e., increasing either of those parameters decreases bubble length while slightly decreasing bubble height as well.

It can be concluded, then, that the integral formulation with strong interaction taken into account and the transition correlation using laminar shear layer parameters provide a good representation of leading-edge bubbles. It should be possible in future studies to use these tools, in conjunction with test data, to investigate and, hopefully, identify the specific mechanism for the breakdown of the bubble. Specifically, systematic analyses of leading-edge bubbles on airfoils under conditions of incipient bubble burst, as indicated by test data, can be carried out to determine whether these bubbles can be characterized by a limiting value of one or more dimensionless shear layer parameters associated with the reattachment process, while at the same time analyzing the turbulent boundary layer just downstream of reattachment to ascertain whether reseparation of the boundary layer occurs.

References

[1]McCullough, G. B. and Gault, D. E., "Examples of Three Representative Types of Airfoil-Section Stall at Low Speed," NACA TN 2502, Sept. 1951.

[2]Ward, J. W., "The Behavior and Effects of Laminar Separation Bubbles on Aerofoils in Incompressible Flow," *Journal of the Royal Aeronautical Society*, Vol. 67, Dec. 1963, pp. 783-790.

[3]Tani, I., "Low-Speed Flows Involving Bubble Separations," *Progress in Aeronautical Science*, Vol. 5, Pergamon Press, New York, 1964, pp. 70-103.

[4]Horton, H. P., "A Semi-Empirical Theory for the Growth and Bursting of Laminar Separation Bubbles," Aeronautical Research Council Current Paper No. 107, June 1967.

[5]Crimi, P. and Reeves, B. L., "A Method for Analyzing Dynamic Stall of Helicopter Rotor Blades," NASA CR 2009, May 1972.

[6]Briley, W. R. and McDonald, H., "Numerical Prediction of Incompressible Separation Bubbles," *Journal of Fluid Mechanics*, Vol. 69, Pt. 4, June 1975, pp. 631-656.

[7]Gault, D. E., "An Experimental Investigation of Regions of Separated Laminar Flow," NACA TN 3505, Sept. 1955.

[8]Tani, I. and Sato, H., "Boundary Layer Transition by Roughness Elements," *Journal of the Physical Society of Japan*, Vol. II, No. 12, Dec. 1956, pp. 1284-1291.

[9]Crimi, P., "Theoretical Study of Dynamic Stall," Avco Systems Div., Wilmington, Mass., Rept. AVSD-0119-74-RR, April 1974.

[10]Lees, L. and Reeves, B. L., "Supersonic Separated and Reattaching Laminar Flows: I. General Theory and Application to Adiabatic Boundary-Layer/Shock-Wave Interactions," *AIAA Journal*, Vol. 2, Nov. 1964, pp. 1907-1920.

[11]Stewartson, K., "Further Solutions of the Falkner-Skan Equation," *Proceedings of the Cambridge Philosophical Society*, Vol. 50, Pt. 3, July 1954, pp. 454-465.

[12]Ojha, S. K., "An Experimental Study of Laminar Separation Bubbles," Indian Institute of Science, Bangalore, India, Rep. AE186/A, April 1967.

[13]Emmons, H. W., "The Laminar-Turbulent Transition in a Boundary Layer," *Journal of Aeronautical Science*, Vol. 18, July 1951, pp. 490-498.

[14]Hunter, L. G. and B. L. Reeves, "Results of a Strong Interaction Wake-Like Model of Supersonic Separated and Reattaching Turbulent Flows," *AIAA Journal*, Vol. 9, No. 4, April 1971, pp. 703-712.

[15]Liepmann, H. W. and Laufer, J., "Investigation of Free Turbulent Mixing," NACA TN 1257, 1947.

[16]Behrens, W., "Separation of a Supersonic Turbulent Boundary Layer by a Forward Facing Step," AIAA Paper 71-127, New York, N.Y., 1971.

[17]Stratford, B. S., "An Experimental Flow with Zero Skin Friction Throughout Its Region of Pressure Rise," *Journal of Fluid Mechanics*, Vol. 5, Jan. 1959, pp. 14-35.

[18]Klineberg, J. and Lees, L., "Theory of Laminar Viscous-Inviscid Interactions in Supersonic Flow," *AIAA Journal*, Vol. 7, Dec. 1969, pp. 2211-2221.